# Predicting layered itinerant magnetic Fe$_3$SiSe$_2$ with spontaneous valley polarization ⊘

Lei Qiao ; Le Fang ✉ ; Qingyun Lv ; Shaowen Xu ; Fanhao Jia ; Wei Wu ; Silvia Picozzi ;
Alexander P. Pyatakov ; Jeffrey R. Reimers ✉ ; Wei Ren ✉

Check for updates

View Online     Export Citation     CrossMark

# Predicting layered itinerant magnetic Fe₃SiSe₂ with spontaneous valley polarization

Lei Qiao,[1,2,3] Le Fang,[1,2,a] Qingyun Lv,[1,2] Shaowen Xu,[1,2] Fanhao Jia,[1,2] Wei Wu,[1,2] Silvia Picozzi,[3] Alexander P. Pyatakov,[4,5] Jeffrey R. Reimers,[1,6,a] and Wei Ren[1,2,a]

## AFFILIATIONS

[1]Physics Department, International Center of Quantum and Molecular Structures, Materials Genome Institute, State Key Laboratory of Advanced Special Steel, Shanghai Key Laboratory of High Temperature Superconductors, Shanghai University, Shanghai 200444, China
[2]Zhejiang Laboratory, Hangzhou 311100, China
[3]Consiglio Nazionale delle Ricerche (CNR-SPIN), Unità di Ricerca presso Terzi c/o Università "G. D'Annunzio," Chieti 66100, Italy
[4]Oscillation Department, Physical Faculty, Lomonosov Moscow State University, Moscow 119991, Russia
[5]MIREA—Russian Technological University, Moscow, 119454, Russia
[6]Department of Mathematical and Physical Sciences, University of Technology Sydney, Ultimo, NSW 2007, Australia

[a]Authors to whom correspondence should be addressed: fangle@shu.edu.cn; Jeffrey.Reimers@uts.edu.au; and renwei@shu.edu.cn

## ABSTRACT

Density functional theory calculations are performed to systematically investigate the electronic and magnetic properties of few-layer and bulk Fe₃SiSe₂ (FSS). We predict that the bulk FSS has a metallic ground state and a layered structure displaying intralayer ferromagnetic ordering and interlayer antiferromagnetic ordering. The itinerant magnetism in the FSS was determined by the Stoner criterion. Predictions of the absence of unstable phonon modes and a moderate cleavage energy of only 28.3 meV/Å² suggest the possibility of stabilizing FSS in a monolayer form. The calculated spin–orbit coupling facilitates not only a large magnetocrystalline anisotropy energy, around $500\,\mu eV/Fe$, but also spontaneous valley polarization in odd-numbered layer systems. These systems have net magnetic moments as the magnetic moments of AFM-ordered layers are not fully compensated in the odd-numbered layer case and are predicted to show 2D metallic behaviors. The magnitude of the valley polarization in odd-numbered layered systems decreases from 18 meV with layer number but is absent in even-layered structures, thus showing an odd–even oscillation effect. Experimental realization of this bidimensional metallic magnet is, therefore, expected to widen the arena of two-dimensional materials that show exotic phenomena.

*Published under an exclusive license by AIP Publishing.* https://doi.org/10.1063/5.0125336

## I. INTRODUCTION

In recent years, great interests have been focused on two-dimensional (2D) magnets for their potential applications in spintronics.[1–4] In particular, identifying various stable layered magnetic materials is the key to a revolution in the design and functionality of devices.[5] In 2017, Cr₂Ge₂Te₆ and CrI₃ were discovered as the first two experimentally synthesized 2D semiconductors with intrinsic magnetism.[1,2] In addition to these, many of the compounds predicted by density functional theory (DFT), such as some layered compounds based on iron and selenium,[6,7] also have exotic properties that promise to expand the family of 2D materials. These are remarkable discoveries as analogous itinerant electron

magnetism in metallic thin films, even approaching the monolayer limit, has been investigated extensively for decades.[8–12] Indeed, such films serve as a testbed for the study of different aspects of 2D magnetism, including the critical behavior and dimensional crossover of magnetic ordering, also of relevance for practical applications in information technology.[13]

Within this context, van der Waals materials offer a class of materials where metallic magnetism can be further investigated. For instance, by focusing on the layered itinerant ferromagnet Fe₃GeTe₂ (FGT), Deng *et al.* demonstrated that its monolayer could present room-temperature ferromagnetism that can be modulated using an ionic gate.[14] The bulk FGT synthesized in the

laboratory was found to have a ferromagnetic (FM) Curie temperature of $T_C = 230$ K.[15] Experimentally, the ground state has been under investigation by means of magnetization characteristics, electrical mobility,[16–18] scanning tunnel microscopy,[19] and magnetic force microscopy,[17] mostly showing a ferromagnetic configuration below the critical temperature. However, Weber et al. observed that the presence of a ferromagnetic amorphous iron germanide impurity over a wide range of synthetic conditions, leading to room-temperature magnetization. Moreover, $Fe_{2.78}GeTe_2$ can still maintain the structure and transition temperature of about 140 K under charge doping and straining.[20]

Deiseroth et al. determined the crystal structure of bulk FGT, revealing an imperfect lattice showing some Fe vacancies, with the chemical formula $Fe_{2.83}GeTe_2$.[15] Its basic structural unit is depicted in Fig. 1, introducing the substitutions $Ge \rightarrow Si$ and $Te \rightarrow Se$ to make FSS; the Wyckoff positions of FGT and FSS and the slight structural difference are listed in Tables SI and SII in the supplementary material. The crystals form layers that stack in the $z$ direction, with each layer of thickness $d_1$ and intralayer separation $d_2$ [Fig. 1(a)]. Their space group is $P6_3/mmc$ (centric $D_{6h}$ point group) with four unique atoms: (i) two symmetry-related Fe atoms named Fe1, (ii) another Fe atom named Fe2, (iii) the Si or Ge atom, and (iv) two symmetry-related Se or Te atoms. Combining with the number of Fe neighbors and bond lengths in Table SII in the



**FIG. 1.** (a) Views of the observed basic structural unit $Fe_3GeTe_2$ of bulk FGT, modified, and optimized to make its analog FSS; Fe1—red, Fe2—yellow, Si—brown, Se—purple; (b) and (c) are the view of monolayer from above and side to show the continuous Fe network as well as Si, we exclude Se in (c). Structural details are presented in Table SII in the supplementary material.

supplementary material, it can be seen that Fe's network is an unusual structure. Each layer contains five atomic planes, with Fe2 and Si or Ge in a central symmetry plane, with planes of Fe1 and then Se or Te atoms on each side. Figure 1 also shows that the vertical stacking forms an AB stacking of layers related internally by both reflection and inversion symmetry operators and, hence, the material has no electrical polarization. It also has no net magnetic moment due to the AFM ordering of inversion symmetry-related magnetic atoms sites. Using the five functionals, as shown in Table SIII in the supplementary material, the energy difference between different stacking and interlayer interactions was calculated, and the ground state of AB stacking and interlayer antiferromagnetic interaction was confirmed.

To understand the current consensus that FGT is ferromagnetic below $T_C$, Jang et al. employed DFT techniques to predict that the ground state of FGT should show the AFM ordering of the layer magnetic moments rather than FM ordering; with a certain concentration of Fe2 defects, the interaction between layers changes from AFM to FM.[21] This result is consistent with the possibility that the vacancies in the Fe2 site in the observed $Fe_{2.83}GeTe_2$ structure lead to FM ordering. Combining the experiments and calculations, Yi et al. proposed that (i) the ground state of FGT should be AFM; (ii) as the temperature raised, FGT experienced a coexistence and competition of FM and AFM phases,[4] and then, a paramagnetic regime is attained at higher temperatures.

The anomalous Hall effect (AHE) occurs in solids with broken time-reversal symmetry, as typical in a ferromagnet. The triangular itinerant ferromagnet FGT single crystal was reported to show anisotropic AHE, when the current is parallel or perpendicular to the van der Waals planes.[22] The AHE of bilayer, trilayer, and multilayer FGT is much stronger than that of the monolayer; furthermore, their AHE can be greatly enhanced by electron doping.[14] Lin and Ni theoretically studied the layer number dependence of the intrinsic anomalous Hall conductivity and found that the bilayer FGT shows the largest value of anomalous Hall conductivity per layer.[23]

Element substitution is one of the most popular ways to expand the search space of materials with desired properties. Hence, we consider the FGT analog FSS, assuming that its structure is analogous. We propose that the FSS is another possible metallic magnet, whose bulk and monolayer structures should be both dynamically stable. Structural, electronic, and magnetic properties are predicted for the bulk and for structures containing from 1 to 9 layers. Intrinsic ferromagnetism is predicted and its origin is discussed from the perspective of the Stoner model.[24] A large magnetocrystalline anisotropy energy (MAE), i.e., $\sim 500\ \mu eV/Fe$, is predicted, quantifying the stabilization of anisotropic magnetism. Upon including spin–orbit coupling (SOC), the odd-numbered few-layer systems are predicted to show valley polarization associated with the number of layers, owing to the presence of net magnetization and inversion symmetry breaking.
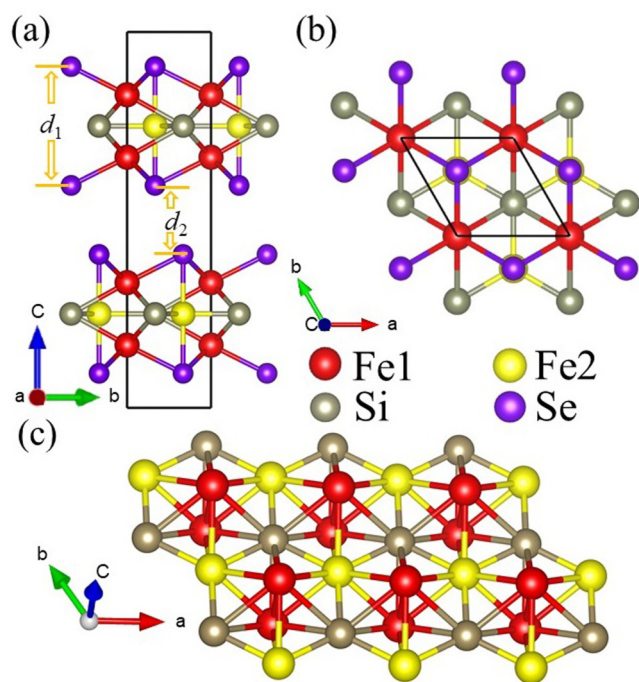
## II. METHOD

DFT simulations were performed within the generalized gradient approximation (GGA)[25] in the form proposed by Perdew–Burke–Ernzerhof (PBE), as implemented in the Vienna Ab initio

Simulation Package (VASP).[26] The long-range van der Waals effects on the structural properties were corrected by using the DFT-D3 method.[27,28] The projector augmented wave (PAW) pseudopotentials[29,30] are used, considering the valence electrons of Fe $3d^6$ $4s^2$, Si $3s^2$ $3p^2$, and Se $4s^2$ $4p^2$. The plane wave energy cutoff was fixed to 600 eV. The convergence criterion of the total energy was set to less than $10^{-6}$ eV, and the maximum force of each ion was less than 0.01 eV/Å. $12 \times 12 \times 4$ and $12 \times 12 \times 1$ $\Gamma$-centered k-grid samplings[31] were adopted for the bulk and 2D systems, respectively. A vacuum space thicker than 15 Å was included to reduce the error from the periodic boundary conditions in 2D systems. The MAE was calculated by taking into consideration SOC.

## III. RESULTS AND DISCUSSIONS

The PBE-D3 optimized structural parameters of bulk and 2D FSS are listed in Table I. The bulk FSS has predicted lattice parameters of $a = b = 3.872$ Å and $c = 15.028$ Å, with $\alpha = \beta = 90°$ and $\gamma = 120°$. The adjacent layers in the bulk have a separation of $d_2 = 2.76$ Å, which is smaller than the value of 2.95 Å obtained in the FGT.[15] We also employed other functionals, resulting in the structural parameters as shown in Table SIV in the supplementary material. The ground state of the bilayer calculated by the PBE functional is FM, and the results of other functionals indicate that the interlayer interaction in the bulk and bilayer is AFM. The calculations predict that the interlayer AB stacking pattern of the bulk is maintained in the multilayer systems. Table SII in the supplementary material lists the optimized Fe–Se and Si–Se bond lengths for the bulk and monolayer systems; these display threefold symmetry, and we manually change the coordinates of the atoms to break the symmetry to mimic the distortion and then do the structural optimization. Finally, the three distortions we set were all eliminated, and the three structures finally returned to the P6₃/mmc space group; hence, no Jahn–Teller distortion is predicted to occur. To neighboring atoms, each Se atom forms 4 bonds, each Si atom 9, each Fe1 atom 10, and each Fe2 atom 11 bonds. This includes some Fe1 − Fe1 and Fe1 − Fe2 bonds that form a continuous network [Fig. 1(c)] of direct iron to iron interactions within each layer. We also manually distorted the structure in three ways to see whether lower-symmetry structures could be stabilized, but the reoptimized structures returned to P6₃/mmc symmetry.

In more detail, the calculated Fe–Fe bond lengths for FSS (Table SII in the supplementary material) are 2.50 Å for Fe1–Fe1 and 2.56 Å for Fe1–Fe2. These are slightly shorter than the values

found in iron metal, 2.87 Å when body-centered cubic and 2.58 Å when face-centered cubic; they are typical of Fe–Fe bond lengths found in coordination compounds, which can show a considerable variation. Each Fe2 atom forms six bonds to Fe1, whereas each Fe1 atom forms only three bonds to Fe2 and one bond to another Fe1. As a result, the iron atoms form a sheet-like continuous topology that runs through the center of each monolayer in the material, but the Fe2 atoms appear to be the most perturbed from simple patterns that could be regarded as depicting metal sheets. The Si and Se atoms sit in and around the iron sheets, forming strong cross-linking bonds [Fig. 1(b)] that stabilize the monolayer structure. The Fe1–Si and Fe1–Se bond lengths are typical of what is expected, whereas the Fe2–Si bond lengths are 0.33 Å shorter than these and the Fe2–Se bond lengths are analogously 0.13 Å shorter. Hence, Fe1 appears to be in a more stable chemical environment than Fe2, and, indeed, calculations performed for the relative energy differences of Fe-site vacancies in FSS predict that the Fe2 vacancy is more stable by 16 meV per cell. This result parallels that known for FGT.[32]

As displayed in Fig. 2(a), the calculated cleavage (binding) energy for a bilayer is $\Delta E_b = 28.3$ meV/Å², which is slightly larger than that of graphite (22.3 meV/Å²)[33] and also nearly two orders of magnitude higher than that of the interlayer AFM coupling (0.46 meV/Å²). The freestanding multilayers are predicted to have slightly larger interlayer distances $d_2$ and layer thickness $d_1$ than in the bulk. Predicted dynamic stability of bulk and monolayer FSS is confirmed by the calculation of the phonon dispersions [Figs. 2(b) and S1 in the supplementary material]. Comparing the phonon dispersion of the monolayer and bulk, it is easy to see that the vibration modes are similar, which also indicates the weak interlayer interaction on the other hand.

The calculated metallic structures of bulk and monolayer FSS are displayed in Fig. 3; these take on metallic natures, as expected from the continuous network of Fe–Fe bonds present in each layer [Fig. 1(c)]. The AFM bulk phase is spin degenerate in the energy bands, while the monolayer shows distinct spin exchange splitting indicative of a ferromagnetic layer. Adjacent layers in the bulk show alternating net spin densities, compensating one with the other to make an interlayer antiferromagnetic ground state. The calculated energy difference between interlayer AFM and interlayer FM spin configurations in the bulk is 2.7 meV/Fe. Interestingly, this value is reduced to 1.0 meV/Fe, when considering a bilayer. The local magnetic moments of each Fe1 and Fe2 atom in bulk FSS are calculated to be $2.45 \mu_B$ and $1.05 \mu_B$, respectively. Most of the

**TABLE I.** The structural parameters (Å), local magnetic moment ($\mu_B$), magnetocrystalline anisotropy energy ($\mu$eV/Fe), and energy difference $E_{AFM–FM}$ (meV/Fe) between antiferromagnetic and ferromagnetic configurations of bulk, bilayer, and monolayer FSS.

| Fe₃SiSe₂ | $a$ (Å) | $d_1$ (Å) | $d_2$ (Å) | $\mu_{Fe1}$ ($\mu_B$) | $\mu_{Fe2}$ ($\mu_B$) | MAE[a] | $E_{AFM–FM}$ |
|---|---|---|---|---|---|---|---|
| Bulk | 3.872 | 4.75 | 2.76 | 2.45 | 1.05 | 447 | −2.7 |
| Bilayer | 3.876 | 4.76 | 2.87 | ±2.51/2.49 | ±1.06 | 465 | −1.0 |
| Monolayer | 3.881 | 4.77 | … | 2.49 | 1.08 | 513 | … |

[a]The MAE is defined by $E = E_{plane} - E_{vertical}$, where $E_{plane}$ and $E_{vertical}$ represent the total energy with the magnetization axis aligned along the in-plane direction and out-of-plane direction, respectively.
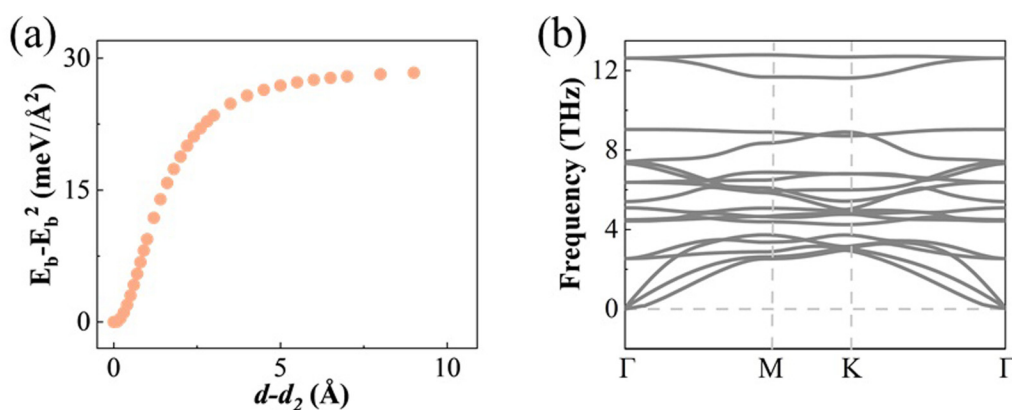
**FIG. 2.** (a) PBE-D3 calculated binding energy changes $\Delta E_b$ for a FSS bilayer as a function of the change in its interlayer spacing $d$–$d_2$ from the bilayer equilibrium value. (b) The PBE calculated phonon dispersion of a monolayer of FSS.

magnetization is localized around the Fe ions, with the Si sites also showing a small contribution due to $d$–$p$ hybridization, and the magnetic moment of Se atoms are almost 0. Additionally, the two equivalent Fe1 sites in the bulk phase are no longer equivalent in the bilayer case since one Fe1 is near the bilayer surface and the other Fe1 is near the interface with the other FSS layer. As a result, the Fe1 sites have two slightly
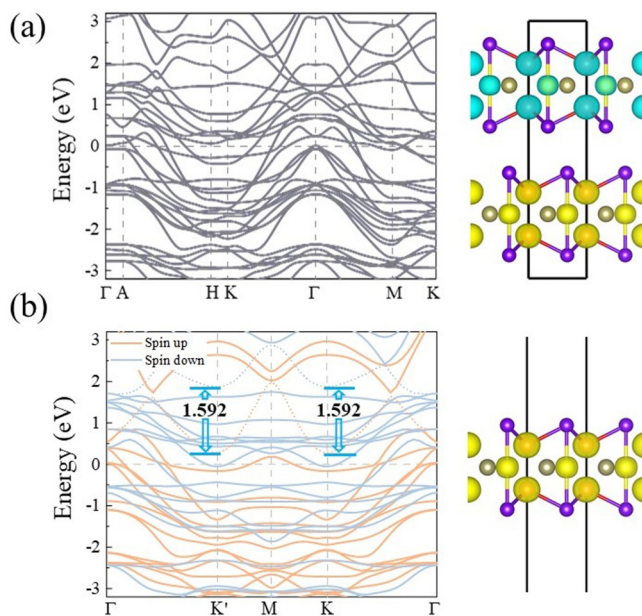


**FIG. 3.** The band structures of (a) AFM bulk and (b) FM monolayer FSS, and the right half is their corresponding spin density (the isosurface value is 0.05 eV/Å³). The dotted lines in (b) are two bands with an equal exchange splitting of 1.592 eV at K and K′.

different values of local moments, namely, $2.49\,\mu_B$ for Fe1 near the surface and $2.51\,\mu_B$ for the other Fe1.

We present the total and projected DOS of bulk and monolayer FSS in Fig. 4. It is easy to see that the contributions of Fe dominate all states nearby the Fermi level. As Fe1 has two equivalent sites in one formula, its weight in the total DOS, as well as its contribution to the spin polarization in the monolayer, is much larger than that of Fe2 sites. The DOS is strongly related to the origin of the itinerant electron magnetism, according to the Stoner model,[24] in which itinerant electrons are treated as a free electron gas. In this model, there are two key parameters: the Stoner parameter $I$ and the density of states at the Fermi level $N(E_F)$ of the non-spin-polarization system. The former parameter describes the strength of the electron exchange, while the latter is inversely proportional to the kinetic energy of the electrons. The competition between the exchange and kinetic energy is considered by the Stoner criterion, namely, a ferromagnetic material needs to have $I \times N(E_F) > 1$. Figure S3 in the supplementary material shows the spin-unpolarized DOS of FSS, which gives a value of $N(E_F) = 1.53$ states/eV per Fe atom and per spin at the Fermi energy.

From fixed spin moment (FSM)[34] calculations, we can estimate the value of the Stoner parameter by fitting the free energy $E$ vs $M$ with a polynomial expansion $E = E_0 + a^\star M^2 + b^\star M^4$, where $a$ is directly related to the Stoner parameter $I$ via $a = 1/N(E_F) - I$ and $M$ is the constrained magnetic moment. As shown in Fig. S3 in the supplementary material, our fit yields $a = -0.67$ eV and $b = 0.16$ eV. By using $N(E_F) = 1.53$ states/eV, the Stoner parameter determined to be 1.32 eV. Therefore, Stoner's criterion of $I \times N(E_F) > 1$ is satisfied, which indicates that ferromagnetism should develop in FSS systems.

On the other hand, long-range magnetic order will be precluded by thermal fluctuations in a low-dimensional isotropic magnetic system according to the Mermin–Wagner theorem.[35] Therefore, to stabilize the 2D ferromagnetic order, the intrinsic MAE is crucial. We find that both the bulk and multilayer FSS show an easy axis in the $c$ direction. The monolayer FSS shows the largest MAE of $513\,\mu$eV/Fe, i.e., about 1.1 times of the value of bulk. These MAE values are also comparable with other previous
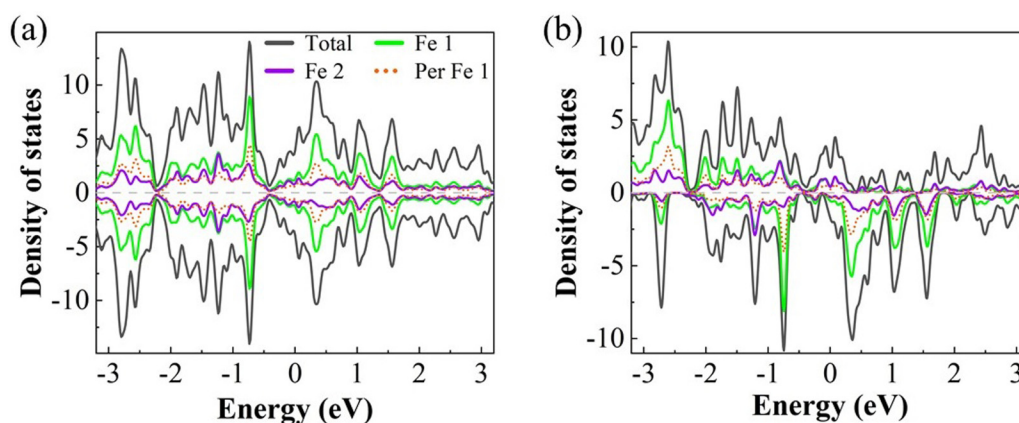
**FIG. 4.** The total density of states (DOS) and the projected DOS to Fe1 and Fe2 of (a) AFM bulk and (b) FM monolayer FSS.

layered magnets, such as VOF[36] and the traditional $3d$ magnets, such as Fe, Co, and Ni.[37]

It is well known that the MAE is originated from the SOC. It leads to many other exotic properties,[38] such as topological order.[39] An interesting phenomenon can be observed when considering SOC in the band structure, as shown in Fig. 5(a). The energetic degeneracy between K and K′ points becomes broken. We define a simple quantity to represent the valley polarization as $\Delta E = E_K - E_{K'}$, which is calculated to be 1.600–1.582 = 0.018 eV for monolayer FSS. This interesting phenomenon is very similar to the spontaneous valley polarization found in LaBr$_2$,[40] and, therefore, it can also be referred to as "valley polarization."

The origin of this phenomenon can be attributed to a combination of inversion symmetry breaking, net spin polarization, and the SOC effect in the FSS monolayer. Specifically, the FSS monolayer belongs to the $C_{3v}$ point group, which is acentric. The absence of

inversion symmetry in the presence of SOC allows by symmetry a spin-splitting at the K and K′ points, though showing opposite spin directions for isoenergetic eigenvalues and, therefore, resulting in the absence of net spin polarization. However, when considering a ferromagnetic spin-configuration, the resulting breaking of time-reversal symmetry allows K and K′ to be no longer degenerate, creating an energy difference that is much smaller than the size of the exchange splitting. We also note that such valley polarization also exists in other materials with the same mechanism, such as monolayer VSi$_2$N$_4$[41] and LaBr$_2$[40] with time reversal and space reversal broken.

To further understand the splitting, we employ a simple model to describe the SOC term as follows[42,43]: $\hat{H}^0_{SOC} + \hat{H}^1_{SOC} = \lambda\hat{L}\hat{S}$, where $\hat{H}^0$ represents the interaction between the same spin states and $\hat{H}^1$ represents the interaction between opposite spin states. $\hat{L}$ and $\hat{S}$ are the orbital angular and spin angular operators, respectively. Because of the FM intralayer
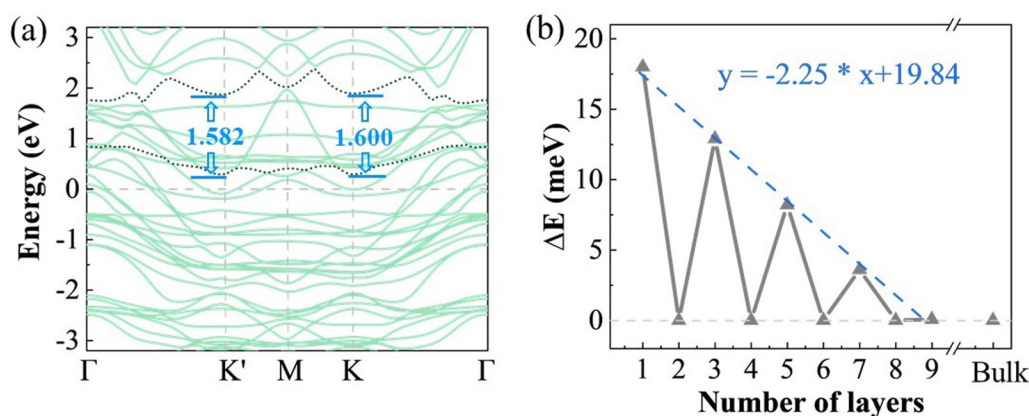


**FIG. 5.** (a) The band structure of monolayer FSS upon including SOC. (b) The energy separation difference $\Delta E$ between K and K′ points, as indicated in (a), as a function of number of FSS layers. The dashed line is a fitted curve and has a slope of −2.25 meV/layer.

interaction, the band would be occupied by only spin-down or spin-up electrons and, therefore, the interactions between opposite spin states will be ignored. $\hat{H}^0$ can be expressed in terms of θ and φ as

$$\hat{H}^0_{SOC} = \lambda \hat{S}_{z'}\left(\hat{L}\cos\theta + \frac{1}{2}\hat{L}_+ e^{-i\phi}\sin\theta + \frac{1}{2}\hat{L}_- e^{+i\phi}\sin\theta\right)$$

by using $(x, y, z)$ and $(x', y', z')$ are the coordinates for $\hat{L}$ and $\hat{S}$, respectively, and setting $\hat{L}_\pm = \hat{L}_x \pm i\hat{L}_y$. Since FSS has an easy axis magnetization, θ is 0. The SOC term can be expressed as $\hat{H}^0_{SOC}(\theta = 0) = \lambda \hat{S}_{z'}\hat{L}_z = \alpha\hat{L}_z$. For monolayer FSS, the K and K′ valleys are dominated by $1e_x$ and $1e_y$ mixed orbitals. Because the group of wave vector K and K′ is $C_{3h}$ and the two wave vectors are connected through time-reversal symmetry, the basic functions at K and K′ valleys can be expressed as $\phi^c_\tau = (1e_x) + (1e_y)$, where $\tau = \pm 1$ denotes the valley. Then, the valley polarization is

$$\Delta E = 2\theta^c_K \downarrow |H|\theta^c_K \downarrow = i(1e_x|\alpha\hat{L}_z|1e_y - 1e_y|\alpha\hat{L}_z|1e_x) = -2\alpha.$$

This model also helps to explain that SOC plays an important role in the spontaneous valley polarization. The valley polarization plays a pivotal role in the creation of valleytronic devices, since it breaks the equivalence between originally identical K and K' valleys, thus effectively increasing the capacity of direct information storage. Moreover, as valley polarization is spontaneous and does not rely on external fields, it circumvents limitations posed by the volatility of such fields. These advantages make FSS an excellent valleytronic material.

Another interesting phenomenon is that $\Delta E$ shows an odd–even layer effect, which, as such, can be controlled by the number of layers. As illustrated in Fig. 5(b), $\Delta E$ is zero when the number of FSS layers is even, whereas it is non-zero when the number of layers is odd. At the same time, the value of $\Delta E$ is linearly decreasing with the increase in odd layer numbers, the slope being $-2.25$ meV/layer. This is a result of the antiferromagnetic coupling between FSS layers and the related absence or presence in the odd or even number of layers, respectively. When the number of layers is odd, the magnetization will produce an equivalent magnetic field, which allows K and K′ to become non-degenerate. On the other hand, in FSS with odd layers (3, 5, 7… layers), the systems maintain the characteristics of the $C_{2v}$ point group. Like $C_{3v}$, $C_{2v}$ is also acentric. When the number of layers increases, due to the thickness effect, $\Delta E$ will decrease. In the case of an even-numbered layer, the point group is $D_{3v}$ (centric point group); hence, the system has no magnetic moment and preserves inversion symmetry; in this case, no equivalent magnetic field is generated, so the degeneracy of K and K′ will not be lifted.

## IV. CONCLUSIONS

In summary, by means of first-principles calculations, we predicted the layered material FSS to be a metallic antiferromagnetic compound with dynamically stable phonon modes. FSS is predicted to show intralayer FM and interlayer AFM couplings in the ground state. The weak interlayer van der Waals-like interaction should allow monolayers of FSS to be exfoliated from the bulk. The Stoner

criterion is predicted to be fulfilled, thereby justifying an itinerant ferromagnetic order in the monolayer. Furthermore, due to its strong SOC effect, monolayer FSS is predicted to exhibit not only a significant MAE of $513\,\mu$eV/Fe but also an intriguing valley polarization in odd-numbered layers, which could be effectively controlled by the FSS layer thickness. Our findings suggest that low-dimensional FSS is a promising candidate suitable for spintronic applications.

In view of its resembling characteristics with FGT, monolayer FSS may also manifest the AHE. Yet, owing to the antiferromagnetic nature of the interlayer interactions in FSS, a distinct layer-number-dependent AHE is likely to be exhibited. In addition, when the AHE meets the spontaneous ferrovalley polarization, a new concept appears, the so-called "anomalous valley Hall effect,"[44] and the study of these properties will provide more perspectives on FSS.

## SUPPLEMENTARY MATERIAL

See the supplementary material for the details of (I) the kinetic stability of FSS, (II) the presentation of the density of states used for the Stoner model, (III) the detailed structure of the FSS including bond lengths and the number of nearest neighbors of each atom, and (IV) similar results from other functional calculations. These data are a supplement to the discussion in the main text.

## AUTHOR DECLARATIONS

### Conflict of Interest

The authors have no conflicts to disclose.

### Author Contributions

**Lei Qiao:** Writing – original draft (equal). **Le Fang:** Writing – review & editing (supporting). **Qingyun Lv:** Writing – review & editing (supporting). **Shaowen Xu:** Writing – review & editing (supporting). **Fanhao Jia:** Writing – review & editing (supporting). **Wei Wu:** Writing – review & editing (supporting). **Silvia Picozzi:** Writing – review & editing (supporting). **Alexander P. Pyatakov:** Writing – review & editing (supporting). **Jeffrey R. Reimers:**

Conceptualization (equal); Supervision (equal); Writing – review & editing (lead). **Wei Ren:** Data curation (equal); Funding acquisition (lead); Investigation (equal); Supervision (lead); Writing – review & editing (equal).

## DATA AVAILABILITY

The data that support the findings of this study are available within the article and its supplementary material.

## REFERENCES

[1]C. Gong, L. Li, Z. L. Li, H. W. Ji, A. Stern, Y. Xia, T. Cao, W. Bao, C. Z. Wang, Y. A. Wang, Z. Q. Qiu, R. J. Cava, S. G. Louie, J. Xia, and X. Zhang, Nature **546**(7657), 265 (2017).

[2]B. Huang, G. Clark, E. Navarro-Moratalla, D. R. Klein, R. Cheng, K. L. Seyler, D. Zhong, E. Schmidgall, M. A. McGuire, D. H. Cobden, W. Yao, D. Xiao, P. Jarillo-Herrero, and X. D. Xu, Nature **546**(7657), 270 (2017).

[3]W. Y. Xing, Y. Y. Chen, P. M. Odenthal, X. Zhang, W. Yuan, T. Su, Q. Song, T. Y. Wang, J. N. Zhong, S. Jia, X. C. Xie, Y. Li, and W. Han, 2D Mater. **4**(2), 7 (2017).

[4]J. Y. Yi, H. L. Zhuang, Q. Zou, Z. M. Wu, G. X. Cao, S. W. Tang, S. A. Calder, P. R. C. Kent, D. Mandrus, and Z. Gai, 2D Mater. **4**(1), 011005 (2016).

[5]L. Zhang, L. Song, H. Dai, J.-H. Yuan, M. Wang, X. Huang, L. Qiao, H. Cheng, X. Wang, W. Ren, X. Miao, L. Ye, K.-H. Xue, and J.-B. Han, Appl. Phys. Lett. **116**(4), 042402 (2020).

[6]A. Bafekry, I. Abdolhosseini Sarsari, M. Faraji, M. M. Fadlallah, H. R. Jappor, S. Karbasizadeh, V. Nguyen, and M. Ghergherehchi, Appl. Phys. Lett. **118**(14), 143102 (2021).

[7]A. Bafekry, M. Faraji, S. Karbasizadeh, I. Abdolhosseini Sarsari, H. R. Jappor, M. Ghergherehchi, and D. Gogova, Phys. Chem. Chem. Phys. **23**(42), 24336 (2021).

[8]J.-U. Lee, S. Lee, J. H. Ryoo, S. Kang, T. Y. Kim, P. Kim, C.-H. Park, J.-G. Park, and H. Cheong, Nano Lett. **16**(12), 7433 (2016).

[9]B. Huang, G. Clark, D. R. Klein, D. MacNeill, E. Navarro-Moratalla, K. L. Seyler, N. Wilson, M. A. McGuire, D. H. Cobden, D. Xiao, W. Yao, P. Jarillo-Herrero, and X. Xu, Nat. Nanotechnol. **13**(7), 544 (2018).

[10]K. Kim, S. Y. Lim, J.-U. Lee, S. Lee, T. Y. Kim, K. Park, G. S. Jeon, C.-H. Park, J.-G. Park, and H. Cheong, Nat. Commun. **10**(1), 345 (2019).

[11]Z. Zhang, J. Shang, C. Jiang, A. Rasmita, W. Gao, and T. Yu, Nano Lett. **19**(5), 3138 (2019).

[12]J. L. Lado and J. Fernandez-Rossier, 2D Mater. **4**(3), 035002 (2017).

[13]C. Huang, J. Feng, F. Wu, D. Ahmed, B. Huang, H. Xiang, K. Deng, and E. Kan, J. Am. Chem. Soc. **140**(36), 11519 (2018).

[14]Y. J. Deng, Y. J. Yu, Y. C. Song, J. Z. Zhang, N. Z. Wang, Z. Y. Sun, Y. F. Yi, Y. Z. Wu, S. W. Wu, J. Y. Zhu, J. Wang, X. H. Chen, and Y. B. Zhang, Nature **563**(7729), 94 (2018).

[15]H. J. Deiseroth, K. Aleksandrov, C. Reiner, L. Kienle, and R. K. Kremer, Eur. J. Inorg. Chem. **2006**, 1561 (2006).

[16]Y. Zhang, H. Y. Lu, X. G. Zhu, S. Y. Tan, W. Feng, Q. Liu, W. Zhang, Q. Y. Chen, Y. Liu, X. B. Luo, D. H. Xie, L. Z. Luo, Z. J. Zhang, and X. C. Lai, Sci. Adv. **4**(1), 8 (2018).

[17]Z. Fei, B. Huang, P. Malinowski, W. Wang, T. Song, J. Sanchez, D. X. Wang Yao, X. Zhu, A. F. May, W. Wu, D. H. Cobden, J.-H. Chu, and X. Xu, Nat. Mater. **17**(9), 778 (2018).

[18]C. Tan, J. Lee, S. G. Jung, T. Park, S. Albarakati, J. Partridge, M. R. Field, D. G. McCulloch, L. Wang, and C. Lee, Nat. Commun. **9**, 1554 (2018).

[19]G. D. Nguyen, J. Lee, T. Berlijn, Q. Zou, S. M. Hus, J. Park, Z. Gai, C. Lee, and A. P. Li, Phys. Rev. B **97**(1), 7 (2018).

[20]D. Weber, A. H. Trout, D. W. McComb, and J. E. Goldberger, Nano Lett. **19**(8), 5031 (2019).

[21]S. W. Jang, H. Yoon, M. Y. Jeong, S. Ryee, H.-S. Kim, and M. J. Han, Nanoscale **12**(25), 13501 (2020).

[22]Y. H. Wang, C. Xian, J. Wang, B. J. Liu, L. S. Ling, L. Zhang, L. Cao, Z. Qu, and Y. M. Xiong, Phys. Rev. B **96**(13), 6 (2017).

[23]X. Q. Lin and J. Ni, Phys. Rev. B **100**(8), 6 (2019).

[24]J. Kübler, *Theory of Itinerant Electron Magnetism* (Oxford University Press, 2017).

[25]J. P. Perdew, K. Burke, and M. Ernzerhof, Phys. Rev. Lett. **77**(18), 3865 (1996).

[26]G. Kresse and J. Hafner, Phys. Rev. B: Condens. Matter **47**(1), 558 (1993).

[27]S. Grimme, J. Antony, S. Ehrlich, and H. Krieg, J. Chem. Phys. **132**(15), 154104 (2010).

[28]S. Grimme, S. Ehrlich, and L. Goerigk, J. Comput. Chem. **32**(7), 1456 (2011).

[29]P. E. Blochl, Phys. Rev. B: Condens. Matter **50**(24), 17953 (1994).

[30]G. Kresse and D. Joubert, Phys. Rev. B **59**(3), 1758 (1999).

[31]H. J. Monkhorst and J. D. Pack, Phys. Rev. B **13**(12), 5188 (1976).

[32]J. Liu, A. Wang, K. Pu, S. Zhang, J. Yang, T. Musho, and L. Chen, Phys. Chem. Chem. Phys. **21**(14), 7588 (2019).

[33]R. Zacharia, H. Ulbricht, and T. Hertel, Phys. Rev. B **69**(15), 155406 (2004).

[34]P. M. Marcus and V. L. Moruzzi, Phys. Rev. B **38**(10), 6949 (1988).

[35]N. David Mermin and H. Wagner, Phys. Rev. Lett. **17**(22), 1133 (1966).

[36]S. Xu, F. Jia, G. Zhao, W. Wu, and W. Ren, J. Mater. Chem. C **9**(29), 9130 (2021).

[37]S. V. Halilov, A. Y. Perlov, P. M. Oppeneer, A. N. Yaresko, and V. N. Antonov, Phys. Rev. B **57**(16), 9557 (1998).

[38]T. Hu, F. Jia, G. Zhao, J. Wu, A. Stroppa, and W. Ren, Phys. Rev. B **97**(23), 235404 (2018).

[39]Z. H. Qiao, W. Ren, H. Chen, L. Bellaiche, Z. Y. Zhang, A. H. MacDonald, and Q. Niu, Phys. Rev. Lett. **112**(11), 116404 (2014).

[40]P. Zhao, Y. Ma, C. Lei, H. Wang, B. Huang, and Y. Dai, Appl. Phys. Lett. **115**(26), 261605 (2019).

[41]X. Zhou, R.-W. Zhang, Z. Zhang, W. Feng, Y. Mokrousov, and Y. Yao, npj Comput. Mater. **7**(1), 160 (2021).

[42]X. Wang, R. Wu, D.-S. Wang, and A. J. Freeman, Phys. Rev. B **54**(1), 61 (1996).

[43]D. Dai, H. Xiang, and M.-H. Whangbo, J. Comput. Chem. **29**(13), 2187 (2008).

[44]W.-Y. Tong, S.-J. Gong, X. Wan, and C.-G. Duan, Nat. Commun. **7**, 13612 (2016).